

LA-UR-18-28408 (Accepted Manuscript)

## Remote homoepitaxy of ZnO microrods across graphene layers

Jeong, Junseok  
Min, Kyung-Ah  
Shin, Dong Hoon  
Yang, Woo Seok  
Yoo, Jinkyung  
Hong, Suklyun  
Hong, Young Joon

Provided by the author(s) and the Los Alamos National Laboratory (2019-04-01).

**To be published in:** Nanoscale

**DOI to publisher's version:** 10.1039/C8NR08084D

**Permalink to record:** <http://permalink.lanl.gov/object/view?what=info:lanl-repo/lareport/LA-UR-18-28408>

**Disclaimer:**

Los Alamos National Laboratory, an affirmative action/equal opportunity employer, is operated by Triad National Security, LLC for the National Nuclear Security Administration of U.S. Department of Energy under contract 89233218CNA000001. By approving this article, the publisher recognizes that the U.S. Government retains nonexclusive, royalty-free license to publish or reproduce the published form of this contribution, or to allow others to do so, for U.S. Government purposes. Los Alamos National Laboratory requests that the publisher identify this article as work performed under the auspices of the U.S. Department of Energy. Los Alamos National Laboratory strongly supports academic freedom and a researcher's right to publish; as an institution, however, the Laboratory does not endorse the viewpoint of a publication or guarantee its technical correctness.

## Trans-epitaxy of ZnO microrods across graphene layers†

Junseok Jeong,<sup>‡a,b,c</sup> Kyung-Ah Min,<sup>‡b,c,d</sup> Dong Hoon Shin,<sup>e</sup> Woo Seok Yang,<sup>f</sup> Jinkyong Yoo,<sup>g</sup> Sang Wook Lee,<sup>e</sup> Suklyun Hong<sup>\*b,c,d</sup> and Young Joon Hong<sup>\*a,b</sup>

<sup>a</sup> Department of Nanotechnology & Advanced Materials Engineering, Sejong University, Seoul 05006, Republic of Korea

E-mail: yjhong@sejong.ac.kr

<sup>b</sup> Graphene Research Institute–Texas Photonics Center International Research Center (GRI–TPC IRC), Sejong University, Seoul 05006, Republic of Korea

<sup>c</sup> Graphene Research Institute, Sejong University, Seoul 05006, Republic of Korea

<sup>d</sup> Department of Physics and Astronomy, Sejong University, Seoul 05006, Republic of Korea

E-mail: hong@sejong.ac.kr

<sup>e</sup> Department of Physics, Ewha Womans University, Seoul 03760, Republic of Korea

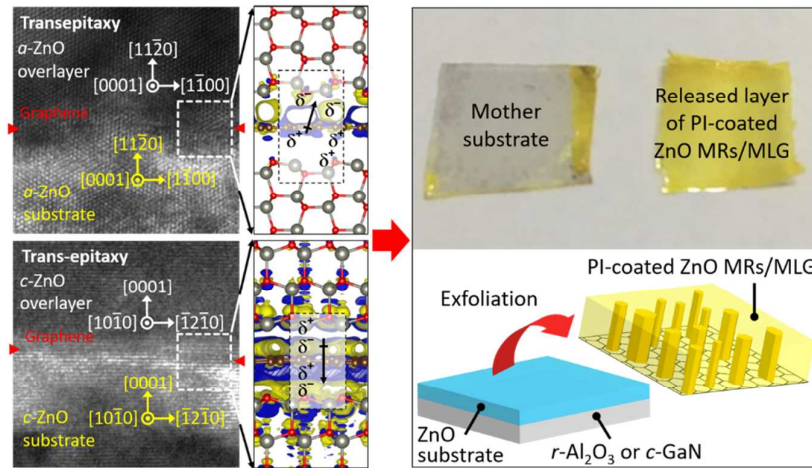
<sup>f</sup> Nano Materials Research Center, Korea Electronics Technology Institute, Seongnam, Gyeonggi-do 13509, Republic of Korea

<sup>g</sup> Center for integrated Nanotechnologies, Los Alamos National Laboratory, Los Alamos, NM 87545, United States

†Electronic supplementary information (ESI) available: Supplementary figures with the details of Raman spectroscopic analysis for graphene layers, cross-sectional transmission electron microscopy images, DFT-calculated atomic structure and charge density difference, scanning electron microscopy images for substrate regeneration.

‡These authors contributed equally to this work

**GRAPHICAL ABSTRACT:** Vertical and horizontal ZnO microrods are grown on *c*- and *a*-plane ZnO across graphene interlayer, owing to charge transfer through graphene, and the trans-epitaxial microrods were exfoliated for substrate regeneration.



**ABSTRACT:** Two-dimensional atomic layered materials (2d-ALMs) have been emerging candidates for the use as epitaxial seed substrates toward transferrable epilayers. However, the micrometer-sized domain of 2d-ALMs precludes the practical use in the epitaxy because of causing crystallographical in-plane disordering of overlayer. Ultrathin graphene can penetrate the electric dipole momentum from underlying crystal layer to graphene surface so that drives to crystallize overlayer at an initial growth stage for substantial energy saving. This study demonstrates the trans-epitaxy of ZnO microrods (MRs) on ZnO substrates across graphene layers via hydrothermal method. Despite of the presence of poly-domain graphene in between ZnO substrate and ZnO MRs, the MRs were epitaxially grown on *a*- and *c*-plane ZnO substrates, whose in-plane alignments were homogeneous within a wafer size. The transmission electron microscopy revealed a homoepitaxial relationship between the overlayer MRs and the substrate. The density-functional theory calculations suggested that the charge redistribution occurring near graphene induces the electric dipole formation, so the attracted adatoms lead to formation of the trans-epitaxial overlayer. Due to a strong potential

field caused by long-range charge transfer given from the substrate, even the use of bi-layer and tri-layer graphene resulted in the trans-epitaxial ZnO MRs. The effect of substrate crystal planes is also theoretically and empirically investigated. The ability of the graphene, which can be released from the mother substrate without covalent bonds, was utilized to transfer the overlayer MR arrays. This method opens a way of producing well aligned, transferrable epitaxial nano/microstructure arrays while regenerating the substrate for cost-saving device manufacturing.

**KEYWORDS:** Epitaxy, graphene, ZnO, hydrothermal growth, density functional theory calculations

## ■ Introduction

Epitaxy, which is a way that crystal growth yields single-crystalline semiconductor films or crystallographically aligned nanostructures on substrates, has been enabled to produce high-performance electronic and optoelectronic devices (e.g., field effect transistors, laser or light-emitting diodes, *etc.*) with high carrier mobility and quantum efficiency.<sup>1-5</sup> Since the conventional epitaxy is achieved by forming strong covalent bonds at the interface between the overlayer and the substrate, the technique limits a choice of substrate materials in terms of a small lattice misfit and single crystallinity to obtain high-quality overlayers with reduced density of an extended crystal defect generating from the interface.<sup>6</sup> After epitaxial growth, the substrate plays important roles in mechanically supporting the overlayer for handling in the post-growth fabrication process, and being the insulation and/or conduction platform for the epitaxial devices to operate the overlayer electronics and optoelectronics. On the contrary, for purposes of economical device production, high-performance device manufacturing, and flexible device fabrication, it is often desirable that the epitaxial overlayers are detached from the substrates via sacrificial layer etching and laser lift-off techniques.<sup>7-9</sup> However, these procedures inevitably involve damage to the overlayer devices, due to the highly corrosive and high photon power-assisted congruent melting conditions required to peel them off from strong covalent bonds<sup>10,11</sup>.

Recently, two-dimensional atomic layered materials (2d-ALMs, *i.e.*, graphene, and hexagonal boron nitride) have been utilized as substrates for semiconductor epitaxy,<sup>1,12-24</sup> and graphene has been highly exploited because of its excellent physical properties, including good electrical and thermal conductivity, high optical transparency, amphoteric *n*- or *p*-type doping, and high elastic modulus<sup>25-29</sup>. Noticeably, the use of van der Waals (vdW)-layered substrates allows overlayer devices transferrable from the mother substrate to various others

of interest through the exfoliation–stamping technique<sup>1,16,30</sup>. More importantly, such transferred devices exhibited no serious degradations in their electrical and electroluminescent properties even after experiencing the repetitive transfer procedures<sup>1,16</sup>, which validated the potential use of 2d-ALM substrates for transferrable, semi-transparent, and flexible device applications.<sup>31,32</sup> Nonetheless, vdW epitaxy of semiconducting materials on 2d-ALMs have been severely hindered by lack of wafer-scale single crystalline 2d-ALM layers as substrates for industrial uses though a few reports of large scale growth of single-domain 2d-ALMs at wafer scale.<sup>33,34</sup>

The limitation of vdW epitaxy<sup>32,35</sup>, due to difficulty in large domain 2d-ALM substrate preparation, can be overcome by a new epitaxy technique reported by Kim *et al.*,<sup>4</sup> demonstrating homoepitaxial single crystalline layers of GaAs(001), InP(001), and GaP(001) over monolayer graphene (MLG) layers on GaAs(001), InP(001), and GaP(001) substrates, respectively, regardless of the graphene domain. Moreover, the heterojunction light-emitting diodes (LEDs) grown on these remote-epitaxially grown (001)-overlayer revealed no degradation in electrical and electroluminescent performances even after exfoliation and the transfer of the LEDs on another substrates, and notably their performances were as good as high-quality LEDs prepared by conventional epitaxy based on covalent bindings between the overlayer and the substrate. This emerging epitaxy technique represented two important scientific findings, which are (i) the crystal structure and orientation is copied from the underlying substrates to the overlayer across ultrathin 2d-ALMs, and (ii) the overlayer can be released and transferred onto an arbitrary substrate without quality degradation. Meanwhile, Chae *et al.* reported about the lattice transparency between the ZnO overlayer and substrate by means of wet chemical synthesis.<sup>36</sup> In particular, from as-grown ZnO polycrystallites/MLG/polycrystalline-ZnO substrate, the crystal structure and the orientation

of overlayer ZnO polycrystallites were found to be the same locally with those of the underlying polycrystalline substrate, which signified that the lattice transparency is valid to copy the more complicated, heterogeneous crystal structures of substrates across MLG. Hence, it further needs to investigate the effect of crystal plane on lattice transparency (or remote epitaxy) for practical applications.

A key characteristic of remote epitaxy and lattice transparency of graphene is distance-dependence of interacting strength between the substrate and the overlayer across 2d-ALM, especially MLG. According to the work by Kim *et al.*, the interaction between GaAs substrate and overgrown GaAs thin film weakens significantly in case of >0.9 nm gap formed by the presence of graphene.<sup>4</sup> To extend the realm of this technique, systematic studies of effects of (i) “physical gap” between substrate and overlayer and (ii) “substrate polarity (or crystal plane)” on interaction that results in the remote epitaxy and the lattice transparency are necessary for diverse materials and applications.

In this paper, we report on hydrothermal trans-epitaxy of the horizontal and vertical ZnO microrods (MRs) on graphene-coated *a*- and *c*-plane ZnO substrates, respectively. The density functional theory (DFT) calculations explore why/how the trans-epitaxy occurred on graphene-coated ZnO substrate. The effects of substrate crystal plane and graphene thickness (or trans-epitaxial gap) on interaction between overlayer and substrate (*i.e.*, adhesion energy, interfacial structural change) are theoretically and experimentally studied. The crystal structures of the trans-epitaxial ZnO MRs/graphene/ZnO substrates are identified using a transmission electron microscopy. In addition, the weakly bound adhesion feature of graphene on the underlying substrate is utilized to transfer the trans-epitaxial MRs overlayer via the simple exfoliation technique, which further enables regeneration of substrates, as well.

## ■ Experimental Section

**Hydrothermal trans-epitaxy and substrate preparation.** ZnO MRs were grown using a nutrient solution of equimolar zinc nitrate hexahydrate [ $\text{Zn}(\text{NO}_3)_2 \cdot 6\text{H}_2\text{O}$ , 25.0 mM] and hexamethylenetetramine [ $\text{C}_6\text{H}_{12}\text{N}_4$ , 25.0 mM] in deionized water at 95 °C for 4 hr in a teflon-lined autoclave (Fig. 1(a)). For the trans-epitaxial substrate preparation, ZnO thin films with a thickness of 5–10 nm were formed by spin-coating a zinc acetate solution [ $\text{C}_4\text{H}_6\text{O}_4\text{Zn} \cdot 2\text{H}_2\text{O}$ , 5.0 mM in ethanol] at 2000 rpm on *r*-plane  $\text{Al}_2\text{O}_3$  ( $10\bar{1}2$ ) and *c*-plane GaN (0001)/ $\text{Al}_2\text{O}_3$  (0001) substrates in order to form *a*-plane ZnO ( $11\bar{2}0$ ) and *c*-plane ZnO (0001) substrates, followed by two-step annealing at 175 and 500 °C for 5 min in an air ambient. This spin-coating step was repeated at least thrice to form heteroepitaxial *a*- and *c*-ZnO substrates with a full coverage of the entire surface of *r*- $\text{Al}_2\text{O}_3$  and *c*-GaN/*c*- $\text{Al}_2\text{O}_3$  substrates, respectively. It is to be noted that the high-temperature annealing enabled the spin-coated thin ZnO layer to be heteroepitaxially crystallized on the original substrates of *c*-GaN and *r*- $\text{Al}_2\text{O}_3$ .<sup>37</sup> For synthesis of the MLG, chemical vapor deposition (CVD) on 35 μm-thick copper foil (Nippon Mining & Metals) was employed, which yielded poly-domain MLG with a typical domain size of 5–20 μm.<sup>38</sup> Then, the MLG was transferred onto the ZnO substrates by the poly(methyl-methacrylate)-supported etching-transfer technique.<sup>39</sup> For coating of multi-layer graphene on substrate, the MLG transfer process was repetitively performed onto the ZnO substrates, which yielded the graphene interlayers with accurate thickness. For bi-layer graphene (BLG) and tri-layer graphene (TLG), two and three MLG sheets were transferred onto the ZnO substrates. The graphene thickness was confirmed using the Raman spectroscopy (Fig. S1†).

**Exfoliation and substrate regeneration.** Prior to exfoliation of MR arrays, the gaps between MRs were filled by spin-coating of polyimide (PI). The PI layer was dried at 120 °C for 2 min, then thermally cured at 300 °C for 5 min. After thermal treatment, the PI-filled MRs overlayer was delaminated from the mother substrate via heat release tape-assisted peeling-off method. The tape was simply removed by heating the released layer at 190 °C. The procedures for exfoliation is schematically depicted in Fig 6(a). The exfoliated substrate was reused for the trans-epitaxy by performing the MLG transfer and hydrothermal growth procedures described in the subsection above.

**Characterizations.** Surface morphologies of the samples were observed by FE-SEM (Hitachi S-4700). The graphene thickness was confirmed by Raman spectroscopic analysis (excitation laser with wavelength of 514 nm and power of 20 mW; Renishaw 2000). Crystal structures of the samples were examined using a HR-TEM (Jeol JEM-ARM 200F) observations and selected area electron diffraction (SAED) analyses. For the HR-TEM observations, samples were cross-sectionally milled with a 30 kV-accelerated beam of gallium ions using a focused ion beam machine (FEI Helios NanoLab<sup>TM</sup>). The incidence electron beam was directed along the ZnO[0001] and  $[10\bar{1}0]$  to determine the crystal structures of the trans-epitaxial ZnO $[11\bar{2}0]$  and [0001] MRs, respectively.

**Computational methods.** The DFT calculations were performed within a generalized gradient approximation (GGA) for the exchange-correlation functionals,<sup>40,41</sup> and were implemented in the Vienna *ab-initio* simulation package (VASP).<sup>42</sup> The kinetic cutoff energy was set to 400 eV, and the projector augmented wave (PAW) potentials were employed to represent the electron-ion interactions.<sup>43</sup> For vdW corrections, Grimme's DFT-D3 method based on a semi-empirical GGA-type theory was adopted.<sup>44</sup> For trans-epitaxial *a*-

ZnO/graphene/*a*-ZnO, ( $4 \times 3$ ) surface unit cell of ZnO ( $11\bar{2}0$ ) and the ( $5 \times 4$ ) rectangular unit cell of graphene were calculated using lattice mismatches of 2.57 and 1.39% in *x*- and *y*-axes, respectively, while the ( $3 \times 3$ ) surface unit cell of oxygen-terminated ZnO (0001) and the ( $4 \times 4$ ) rhombic unit cell of graphene were calculated using lattice mismatch of 0.91% between them for trans-epitaxial *c*-ZnO/graphene/*c*-ZnO. Regarding the Brillouin zone integration, ( $2 \times 3 \times 1$ ) grid for *a*-ZnO/graphene/*a*-ZnO and ( $3 \times 3 \times 1$ ) grid for *c*-ZnO/graphene/*c*-ZnO were used in the Gamma centred scheme. The atomic configurations were fully optimized as long as the Hellmann–Feynman forces became less than  $0.02 \text{ eV } \text{\AA}^{-1}$ . The charge density difference ( $\Delta\text{CD}$ ) was determined by the expression  $\Delta\text{CD}_{\text{graphene/ZnO}} = n_{\text{graphene/ZnO}} - (n_{\text{graphene}} + n_{\text{ZnO}})$ , where  $n_{\text{graphene/ZnO}}$ ,  $n_{\text{graphene}}$ , and  $n_{\text{ZnO}}$  are charge densities of graphene/ZnO, graphene, and ZnO, respectively. For the graphene-coated ZnO substrates, the  $\Delta\text{CD}$  of the trans-epitaxial heterointerfaces was also calculated using  $\Delta\text{CD}_{\text{ZnO/graphene/ZnO}} = n_{\text{ZnO/graphene/ZnO}} - (n_{\text{ZnO(overlayer)}} + n_{\text{graphene/ZnO}})$ , where  $n_{\text{ZnO/graphene/ZnO}}$ ,  $n_{\text{ZnO(overlayer)}}$ , and  $n_{\text{graphene/ZnO}}$  are charge densities of ZnO/graphene/ZnO, ZnO overlayer, and graphene/ZnO substrate, respectively.

## ■ Results and Discussion

As depicted in Fig. 1(a), trans-epitaxy was performed via hydrothermal growth of ZnO MRs on graphene-coated *a*- and *c*- plane ZnO substrates. Figs. 1(b) and (c) schematically represent the surface morphologies of trans-epitaxial ZnO MR arrays grown on MLG-coated *a*- and *c*-ZnO substrates, respectively. Intriguingly, although ZnO MRs were grown on the same smooth, clean MLG surface (insets in Figs. 1(d) and (e)) under the same hydrothermal growth conditions, even in the same batch, two templates of the MLG/*a*-ZnO and the MLG/*c*-ZnO yielded two different overlayer morphologies of horizontally and vertically aligned MR

arrays, respectively (Figs. 1(d) and (e)). Noticeably, these MRs were found to be well aligned with good in-plane ordering of unidirectional horizontal arrays (Fig. 1(d)) and a uniform six-fold rotational alignment of vertical MR sidewall  $\{\bar{1}100\}$  facets (indicated with arrows in Fig. 1(e)) by plan-view field-emission scanning electron microscope (FE-SEM) observations. This suggests the existence of specific epitaxial relationships between MRs and ZnO substrates.

The cross-sectional FE-SEM image of a single horizontal ZnO MR, shown at the bottom panel of Fig. 1(d), clearly exhibits a lying-down morphology of the prismatic rod with facets of  $\{\bar{1}100\}$  *m*-planes (red and green colored) and (0001) *c*-plane (blue colored) of wurtzite, whose body is cut in half along the *a*-plane, parallel to the substrate surface. These morphological features were identically observed from other horizontal MRs as well. As displayed in Fig. 1(e), MR arrays grown on MLG/*c*-ZnO show the vertical alignment without exception.

If the MLG surface as a seed layer offered the epitaxial relationship, the homogeneous alignments of MR arrays could not be achieved in such a long range over the entire substrate area because the mean domain size of the CVD-grown graphene is typically a few  $\mu\text{m}$ . Hence, such long-range morphological ordering of as-grown MRs shown in Fig. 2 is tentatively associated with single crystallinity of the ZnO substrates even though the poly-domain graphene is covered on the substrates. It is worth noting that the MLG was not damaged after the hydrothermal growth of the ZnO because of the low temperature and the mild growth condition, which was confirmed by the Raman spectroscopic analysis (Fig. S2<sup>†</sup>).

Crystal structures and epitaxial relationships of the ZnO MR/MLG/ZnO substrate were examined using a high-resolution transmission electron microscope (HR-TEM). Fig. 3(a) displays the cross-sectional HR-TEM image taken around the heterointerfaces of the

horizontal ZnO MR/MLG/*a*-ZnO (on *r*-Al<sub>2</sub>O<sub>3</sub>), which showed the structural discontinuity, as indicated by red arrows, because of the MLG existence between the *a*-ZnO overlayer and the substrate. Two lattice images of the overlayer and the substrate in Fig. 3(b) clearly demonstrate the identical lattice arrangements of the ZnO MR overlayer and the substrate. Considering the lattice constants of ZnO ( $a = b = 3.249 \text{ \AA}$ ;  $c = 5.206 \text{ \AA}$  for wurtzite), those lattice images represent a trans-epitaxial relationship of  $(11\bar{2}0)[0001]_{\text{overlayer}} \parallel (11\bar{2}0)[0001]_{\text{substrate}}$  across the MLG. Also, the SAED patterns also identified the aforementioned trans-epitaxial relationship (Fig. 3(c)), without no other irregular diffraction spots caused from the ZnO. This indicates a single crystallinity of the trans-epitaxial *a*-ZnO overlayer/*a*-ZnO substrate. The diffraction patterns also corroborate that the *a*-ZnO substrate was heteroepitaxially grown on *r*-Al<sub>2</sub>O<sub>3</sub> with a relationship of  $(11\bar{2}0)[0001]_{\text{ZnO substrate}} \parallel (1\bar{1}02)[\bar{1}101]_{r\text{-sapphire}}$ .

In Figs. 3(d) and (e), the same *c*-axial crystallographic orientations of the wurtzite ZnO overlayer and substrate are displayed, which were taken from the vertical ZnO MR/MLG/*c*-ZnO (on *c*-GaN). The lattice orientations of the *c*-ZnO overlayer and substrate were found to be well matched and aligned, which indicated the trans-epitaxial  $(0001)[10\bar{1}0]_{\text{overlayer}} \parallel (0001)[10\bar{1}0]_{\text{substrate}}$  relationship. The interplanar spacings between adjacent lattice planes in both the ZnO overlayer and substrate were measured to be  $2.59 \text{ \AA}$  that corresponds to the *d*-spacing of ZnO (0002). As shown in Fig. 3(f), the SAED patterns reveal the epitaxial  $(0001)[10\bar{1}0]_{\text{MR}} \parallel (0001)[10\bar{1}0]_{\text{ZnO substrate}} \parallel (0001)[10\bar{1}0]_{\text{GaN}}$  relationship, and noticeably the trans-epitaxial relationship was well maintained even with the use of thicker graphene interlayers of BLG or TLG (Fig. S3†).

The DFT calculations were conducted to explore how/why the trans-epitaxy of the ZnO overlayer was made possible across graphene layers. The stable molecular structures were simulated, and charge transfer (or redistribution) at the heterointerface was estimated by calculating  $\Delta CD$  for the substrate and trans-epitaxial structures. The left panel of Fig. 4(a) shows the calculated structure of MLG adheres to an *a*-ZnO substrate with the equilibrium vdW gap of 2.95 Å and adhesion energy of  $-21.5 \text{ meV \AA}^{-2}$  for the MLG/*a*-ZnO substrate before the overlayer growth, and the charge transfer mostly occurs at the graphene/*a*-ZnO interface. Though the electron ( $e^-$ ) accumulation and depletion appear alternately along the MLG side within the non-covalent binding gap,  $e^-$  depletion is slightly predominant around the MLG and the surface of MLG shows  $e^-$  depleted surface. Only a small amount of  $e^-$  accumulation remains at the *a*-ZnO substrate. Hence, as depicted in inset of Fig. 4(a), the charge redistribution at the vdW binding interface possibly makes electric dipole (or bond dipole) with a vertical directional component. Intriguingly, the slight lattice buckling was simulated on both sides. In particular, interfacial oxygen ions protrude toward the graphene, which possibly breaks the perfect non-polar symmetry of the wurtzite *a*-plane. As a result, the  $e^-$  depletion becomes slightly dominant at the substrate side with a net positive charge, which develops electric dipoles with a normal direction component (inset of Fig. 4(a)). This leads to the diffuse-in and adhesion of precursor adatoms, followed by nucleation–epitaxy.

The right panel of Fig. 4(a) shows the trans-epitaxial *a*-ZnO/MLG/*a*-ZnO heterointerfaces, displaying that the  $\Delta CD$  appears at the overlayer/MLG interface, tentatively due to charge transfer. Such charge redistribution makes the strong bond dipoles with vertical direction component at the overlayer/MLG interface, as depicted in dot-line box of right panel in Fig. 4(a). The equilibrium spacings of the overlayer–MLG and MLG–substrate are 2.89 and 2.88 Å, respectively, and the adhesion energy of overlayer–(MLG-coated substrate)

was estimated to be  $-24.5 \text{ meV } \text{\AA}^{-2}$ . It should be noted that the spacing of the MLG–substrate becomes smaller with decreased adhesion energy after the trans-epitaxy, presumably due to the strong attraction between the overlayer and substrate across graphene.

Meanwhile, in the MLG/*c*-ZnO substrate (left panel of Fig. 4(b)), the  $e^-$  depletion dominantly appears along the adhered MLG side while electrons are accumulated on the *c*-ZnO substrate, which lead to formation of vertical electric dipoles. The adhesion energy of MLG on *c*-ZnO was  $-31.3 \text{ meV } \text{\AA}^{-2}$  with a gap distance of  $3.12 \text{ \AA}$ . After the growth of the overlayer (right panel of Fig. 4(b)), the  $\Delta\text{CD}$  additionally appears at the overlayer/MLG interface (dot-line box), implying that the attraction from the substrate transferred to the overlayer across graphene. For the trans-epitaxial structure, the spacings of the overlayer–MLG and MLG–substrate are calculated to be  $2.69$  and  $2.78 \text{ \AA}$ , respectively, and the adhesion energy of the overlayer to MLG is  $-52.0 \text{ meV } \text{\AA}^{-2}$ . We noted that the spacing of the MLG–*c*-ZnO substrate is significantly reduced from  $3.12$  to  $2.78 \text{ \AA}$  after trans-epitaxy, due to the strong electrostatic attraction carried through the vertical dipoles between the overlayer and substrate. The smaller calculated gap distance of  $5.47 \text{ \AA}$  between overlayer and substrate in the *c*-axial trans-epitaxial structure than that in the *a*-axial one ( $5.77 \text{ \AA}$ ) support the crucial role of substrate polarity in more energetically stable trans-epitaxial structures with a substantial energy saving and stronger attraction between overlayer and substrates.

The trans-epitaxial *c*-ZnO/BLG/*c*-ZnO structures were further calculated to examine the effect of the graphene thickness (or trans-epitaxial gap) on  $\Delta\text{CD}$  and the heterointerfacial structure. Fig. 4(c) exhibits that the top of the *c*-ZnO substrate and the surface of the BLG are oppositely charged before trans-epitaxy, and in between them charge accumulation and depletion regions alternately forms, which results in formation of vertical dipoles. After trans-epitaxy, the  $\Delta\text{CD}$  predominantly appears between the top of the BLG and the bottom of the *c*-

ZnO with adhesion energy of  $-32.3 \text{ meV } \text{Å}^{-2}$ , whose absolute value is much smaller than that of the *c*-ZnO on MLG/*c*-ZnO, because of increased gap between the overlayer and substrate. Thus, the use of thicker graphene reduces the adhesion of overlayer due to the wider physical gap between the overlayer and substrate. The DFT-calculated results imply that the amount of net charge difference (or the amount of charge transfer) along the *z*-axis plays an important role in determining both the equilibrium distance and the adhesion energy of the overlayer-graphene (see also Fig. S4† for charge redistribution at isosurface levels of  $\pm 0.001 \text{ e/bohr}^3$ ). In practice, the use of polar *c*-ZnO and/or thinner graphene (or trans-epitaxial gap) is surmised to induce a stronger attraction between substrate and adatoms adhered onto graphene surface, which possibly facilitates the enhanced nucleation of the overlayer.<sup>45</sup>

In this regard, the impact of the trans-epitaxial gap was empirically investigated by growing MRs on graphene-coated ZnO substrates with different graphene thicknesses (e.g., MLG, BLG, and TLG-coated substrates). Fig. 5 displays the number density of trans-epitaxial MRs plotted as a function of graphene thickness. Overall, the MR number density was decreased with increase of graphene thickness because of the dipole momentum damping as a function of trans-epitaxial gap. For instance, when using an *a*-ZnO substrate (Fig. 5(a)), the number density was reduced from  $9.8 \times 10^3$  to  $1.4 \times 10^3 \text{ mm}^{-2}$  as increasing the graphene thickness from MLG to TLG; for the use of *c*-ZnO substrate (Fig. 5(b)),  $1.7 \times 10^5$  to  $2.2 \times 10^4 \text{ mm}^{-2}$ . It should be also noted that the use of the *c*-ZnO substrate yielded a much higher MR number density than the *a*-ZnO under the same gap conditions. This result identifies that a higher field strength with a polar substrate and/or a narrower gap is crucial to form trans-epitaxial nano/microstructures of higher density.

Exfoliation of the trans-epitaxial ZnO MRs overlayer was carried out to adopt the ability of graphene to be readily released from substrate, because of the weakly bound vdW bonds to

the mother substrate surface. We particularly attempted the release of vertical MRs with a high aspect ratio of  $\sim 6$ . For the overlayer exfoliation, PI was spin-coated between MRs. The PI-supported MRs overlayer was then delaminated from the mother substrate using the heat release tape that can be removed by heating on a hot plate. A series of schematics and photographs in Fig. 6(a) exhibits the exfoliation procedures and the corresponding resultant products, respectively. The SEM image of Fig. 6(b), taken from released side of PI-coated MR arrays, shows a smooth bottom finish of *c*-ZnO MRs. Furthermore, the surface of the remained *c*-ZnO substrate after the release was found to be quite smooth and clean (inset of Fig. 6(b)). This signifies that the bottom of ZnO MRs overlayer was completely released from the mother substrate.

The location of graphene after exfoliation was confirmed using Raman spectroscopy (Fig. 6(c)). Before the exfoliation, the ZnO MRs/graphene/ZnO substrate exhibited graphene-associated peaks, which are D, G, and 2D, at 1347, 1572, and 2669  $\text{cm}^{-1}$ , respectively. However, after exfoliation, these peaks were not observed on the mother substrate but on the released backside of the PI-coated MRs overlayer. This indicates that the graphene was completely removed together with the MRs overlayer from the mother substrate using the simple mechanical tape-release technique. According to the work by Kim *et al.*, the graphene interlayer remains on the substrate after release of a thin film overlayer,<sup>4</sup> which is different from our result that the graphene is transferred in conjunction with the overlayer. We surmise that either the use of a sticky, adhesive gap filler PI or a stronger adhesion between the graphene and the overlayer (Fig. 4) facilitated the delamination of the overlayer/graphene from the mother substrate.

The successful exfoliation was extended to the regeneration of the used ZnO substrate. The mother substrates after the exfoliation were reused by repeating the procedures of graphene

transfer and hydrothermal growth of ZnO MRs which are shown in Fig. 1(a). Fig. 7 displays that the reuse of mother substrates with MLG interlayer produced the trans-epitaxial MR arrays whose morphologies and number densities (within a deviation of  $\pm 10\%$ ) are almost same with those grown on the virgin substrates. For the use of BLG and TLG interlayers, the reused mother substrates yielded well aligned MR arrays as well (Fig. S5<sup>†</sup>). This indicated that the substrates can be reliably reused for cost-saving production of the transferable MR arrays.

## ■ Conclusion

In summary, we have demonstrated the trans-epitaxy of ZnO MRs using graphene-coated ZnO substrates with different trans-epitaxial gaps and substrate crystal planes. Both the *a*- and *c*-plane ZnO substrates, which correspond to apolar and polar surfaces, respectively, yielded horizontal and vertical MR arrays with homogeneous in-plane alignment, because of homoepitaxial relationship across graphene. As increasing the trans-epitaxial gap with use of thicker graphene, the number density of MRs was significantly decreased, and polar substrate resulted in higher density MR arrays. These experimental results corroborate our argument that stronger electric dipole momentum along *z*-direction from the substrate side can be well transferred through thinner graphene, which eventually attracts more adatoms for higher density formation of MRs. According to DFT calculations, the electric dipole (or potential field) induced via charge redistribution by junction of graphene/substrate played an important role for trans-epitaxy. Strong attraction between overlayer and substrate resulted in decreased interplanar spacings with substantial adhesion energy savings. Moreover, the attraction was calculated to be strongly affected by both the gap distance and substrate crystal plane, which elucidates why polar and smaller gaps

produced higher density MR arrays. We surmise that the vdW heterointerface and graphene without permanent dipoles enabled the penetration of induced dipoles formed at the graphene/substrate junction across graphene layers. Our complementary theoretical and experimental results provide fundamental insights for understanding the ability of graphene layers that penetrate the electric dipole momentum for trans-epitaxy. More importantly, we showed that the use of multilayer graphene (e.g., BLG and TLG) is possible to obtain trans-epitaxial MR arrays on both polar and apolar substrates for the first time. For practical applications, the vdW binding of graphene to the substrate presented important implications for release of MRs overlayer and reuse of substrates. Hence, we anticipate that this promising method could be readily applied to fabricate more materials and diverse devices that are transferrable from regenerated substrates on demands.

### **Conflicts of interest**

There are no conflicts of interest to declare.

### **Acknowledgement**

This research was financially supported by the Basic Science Research Programs (NRF-2016R1D1A1B03931518; NRF-2015R1A2A2A05050829; NRF-2017R1A2B2010123), Priority Research Center Program (2010-0020207) and International Research Center Program (2018K1A4A3A01064272) through the NRF of Korea. The authors gratefully acknowledge financial support of the KIAT through the International Cooperative R&D program (N0001819). This work was performed in part at CINT, a U.S. Department of

Energy, office of Basic Energy Sciences User Facility at Los Alamos National Laboratory (Contract DE-AC52-06NA25396) and Sandia National Laboratories (Contract DE-AC04-94AL85000).

## ■ REFERENCES

1. K. Chung, C. H. Lee and G. C. Yi, *Science*, 2010, **330**, 655–657.
2. Y. J. Hong, C. H. Lee, A. Yoon, M. Kim, H. K. Seong, H. J. Chung, C. Sone, Y. J. Park and G. C. Yi, *Adv. Mater.*, 2011, **23**, 3284–3288.
3. K. Tomioka, M. Yoshimura and T. Fukui, *Nature*, 2012, **488**, 189–192.
4. Y. Kim, S. S. Cruz, K. Lee, B. O. Alawode, C. Choi, Y. Song, J. M. Johnson, C. Heidelberger, W. Kong, S. Choi, K. Qiao, I. Almansouri, E. A. Fitzgerald, J. Kong, A. M. Kolpak, J. Hwang and J. Kim, *Nature*, 2017, **544**, 340–343.
5. S. Gazibegovic, D. Car, H. Zhang, S. C. Balk, J. A. Logan, M. W. A. de Moor, M. C. Cassidy, R. Schmits, D. Xu, G. Z. Wang, P. Krogstrup, R. Veld, K. Zuo, Y. Vos, J. Shen, D. Bouman, B. S. Hojatei, D. Pennachio, J. S. Lee, P. J. van Veldhoven, S. Koelling, M. A. Verheijen, L. P. Kouwenhoven, C. J. Palmstrom and E. Bakkers, *Nature*, 2017, **548**, 434–438.
6. J. E. Ayers, *Heteroepitaxy of semiconductor: Theory, Growth, and Characterization*, CRC Press, Boca Raton, FL, Boca Raton, FL, 1st edn., **2007**.
7. W. S. Wong, T. Sands, N. W. Cheung, M. Kneissl, D. P. Bour, P. Mei, L. T. Romano and N. M. Johnson, *Appl. Phys. Lett.*, 1999, **75**, 1360–1362.
8. J. Yoon, S. Jo, I. S. Chun, I. Jung, H. S. Kim, M. Meitl, E. Menard, X. L. Li, J. J. Coleman, U. Paik and J. A. Rogers, *Nature*, 2010, **465**, 329–333.
9. C. W. Cheng, K. T. Shiu, N. Li, S. J. Han, L. Shi and D. K. Sadana, *Nat. Commun.*, 2013, **4**, 1577.
10. J. H. Cheng, Y. S. Wu, W. C. Peng and H. Ouyang, *J. Electrochem. Soc.*, 2009, **156**, H640–H643.
11. M. H. Doan, S. Kim, J. J. Lee, H. Lim, F. Rotermund and K. Kim, *AIP Adv.*, 2012, **2**, 022122.
12. J. M. Lee, Y. B. Pyun, J. Yi, J. W. Choung and W. I. Park, *J. Phys. Chem. C*, 2009, **113**, 19134–19138.
13. Y. J. Kim, J. H. Lee and G. C. Yi, *Appl. Phys. Lett.*, 2009, **95**, 213101.
14. Y. J. Hong and T. Fukui, *ACS Nano*, 2011, **5**, 7576–7584.
15. Y. J. Hong, W. H. Lee, Y. P. Wu, R. S. Ruoff and T. Fukui, *Nano Lett.*, 2012, **12**, 1431–1436.
16. Y. Kobayashi, K. Kumakura, T. Akasaka and T. Makimoto, *Nature*, 2012, **484**, 223–227.
17. A. M. Munshi, D. L. Dheeraj, V. T. Fauske, D. C. Kim, A. T. J. van Helvoort, B. O. Fimland and H. Weman, *Nano Lett.*, 2012, **12**, 4570–4576.
18. K. Chung, S. I. Park, H. Baek, J. S. Chung and G. C. Yi, *NPG Asia Mater.*, 2012, **4**, e24.
19. P. K. Mohseni, A. Behnam, J. D. Wood, C. D. English, J. W. Lyding, E. Pop and X. L. Li, *Nano Lett.*, 2013, **13**, 1153–1161.

20. A. M. Munshi and H. Weman, *Phys. Status Solidi RRL*, 2013, **7**, 713–726.
21. Y. J. Hong, J. W. Yang, W. H. Lee, R. S. Ruoff, K. S. Kim and T. Fukui, *Adv. Mater.*, 2013, **25**, 6847–6853.
22. J. Wallentin, D. Kriegner, J. Stangl and M. T. Borgstrom, *Nano Lett.*, 2014, **14**, 1707–1713.
23. P. K. Mohseni, A. Behnam, J. D. Wood, X. Zhao, K. J. Yu, N. C. Wang, A. Rockett, J. A. Rogers, J. W. Lyding, E. Pop and X. L. Li, *Adv. Mater.*, 2014, **26**, 3755–3760.
24. K. Chung, H. Beak, Y. Tchoe, H. Oh, H. Yoo, M. Kim and G. C. Yi, *APL Mater.*, 2014, **2**, 092512.
25. A. A. Balandin, S. Ghosh, W. Z. Bao, I. Calizo, D. Teweldebrhan, F. Miao and C. N. Lau, *Nano Lett.*, 2008, **8**, 902–907.
26. C. Lee, X. D. Wei, J. W. Kysar and J. Hone, *Science*, 2008, **321**, 385–388.
27. D. C. Wei, Y. Q. Liu, Y. Wang, H. L. Zhang, L. P. Huang and G. Yu, *Nano Lett.*, 2009, **9**, 1752–1758.
28. X. S. Li, W. W. Cai, J. H. An, S. Kim, J. Nah, D. X. Yang, R. Piner, A. Velamakanni, I. Jung, E. Tutuc, S. K. Banerjee, L. Colombo and R. S. Ruoff, *Science*, 2009, **324**, 1312–1314.
29. S. Bae, H. Kim, Y. Lee, X. F. Xu, J. S. Park, Y. Zheng, J. Balakrishnan, T. Lei, H. R. Kim, Y. I. Song, Y. J. Kim, K. S. Kim, B. Ozyilmaz, J. H. Ahn, B. H. Hong and S. Iijima, *Nat. Nanotech.*, 2010, **5**, 574–578.
30. J. Kim, C. Bayram, H. Park, C. W. Cheng, C. Dimitrakopoulos, J. A. Ott, K. B. Reuter, S. W. Bedell and D. K. Sadana, *Nat. Commun.*, 2014, **5**, 4836.
31. C. H. Lee, Y. J. Kim, Y. J. Hong, S. R. Jeon, S. Bae, B. H. Hong and G. C. Yi, *Adv. Mater.*, 2011, **23**, 4614–4619.
32. Y. J. Hong and C. H. Lee, in *Semiconductor Nanowires I: Growth and Theory*, eds. A. F. I. Morral, S. A. Dayeh and C. Jagadish, Academic Press, Burlington, **2015**, vol. 93, ch. 3, pp. 125–172.
33. J. H. Lee, E. K. Lee, W. J. Joo, Y. Jang, B. S. Kim, J. Y. Lim, S. H. Choi, S. J. Ahn, J. R. Ahn, M. H. Park, C. W. Yang, B. L. Choi, S. W. Hwang and D. Whang, *Science*, 2014, **344**, 286–289.
34. X. Z. Xu, Z. H. Zhang, J. C. Dong, D. Yi, J. J. Niu, M. H. Wu, L. Lin, R. K. Yin, M. Q. Li, J. Y. Zhou, S. X. Wang, J. L. Sun, X. J. Duan, P. Gao, Y. Jiang, X. S. Wu, H. L. Peng, R. S. Ruoff, Z. F. Liu, D. P. Yu, E. G. Wang, F. Ding and K. H. Liu, *Sci. Bull.*, 2017, **62**, 1074–1080.
35. H. Yoo, K. Chung, Y. S. Choi, C. S. Kang, K. H. Oh, M. Kim and G. C. Yi, *Adv. Mater.*, 2012, **24**, 515–518.
36. S. Chae, S. H. Jang, W. J. Choi, Y. S. Kim, H. J. Chang, T. I. Lee and J. O. Lee, *Nano Lett.*, 2017, **17**, 1711–1718.
37. L. E. Greene, M. Law, D. H. Tan, M. Montano, J. Goldberger, G. Somorjai and P. D. Yang, *Nano Lett.*, 2005, **5**, 1231–1236.
38. D. S. Choi, K. S. Kim, H. Kim, Y. Kim, T. Kim, S. H. Rhy, C. M. Yang, D. H. Yoon and W. S. Yang, *ACS Appl. Mater. Interfaces*, 2014, **6**, 19574–19578.
39. K. S. Kim, Y. Zhao, H. Jang, S. Y. Lee, J. M. Kim, K. S. Kim, J. H. Ahn, P. Kim, J. Y. Choi and B. H. Hong, *Nature*, 2009, **457**, 706–710.
40. W. Kohn and L. J. Sham, *Phys. Rev.*, 1965, **140**, A1133–A1138.
41. J. P. Perdew, K. Burke and M. Ernzerhof, *Phys. Rev. Lett.*, 1996, **77**, 3865–3868.
42. G. Kresse and J. Furthmuller, *Phys. Rev. B*, 1996, **54**, 11169–11186.
43. G. Kresse and D. Joubert, *Phys. Rev. B*, 1999, **59**, 1758–1775.
44. S. Grimme, J. Antony, S. Ehrlich and H. Krieg, *J. Chem. Phys.*, 2010, **132**, 154104.

45. J. Yoo, T. Ahmed, R. J. Chen, A. P. Chen, Y. H. Kim, K. C. Kwon, C. W. Park, H. S. Kang, H. W. Jang, Y. J. Hong, W. S. Yang and C. H. Lee, *Nanoscale*, 2018, **10**, 5689–5694.

## Figures and captions

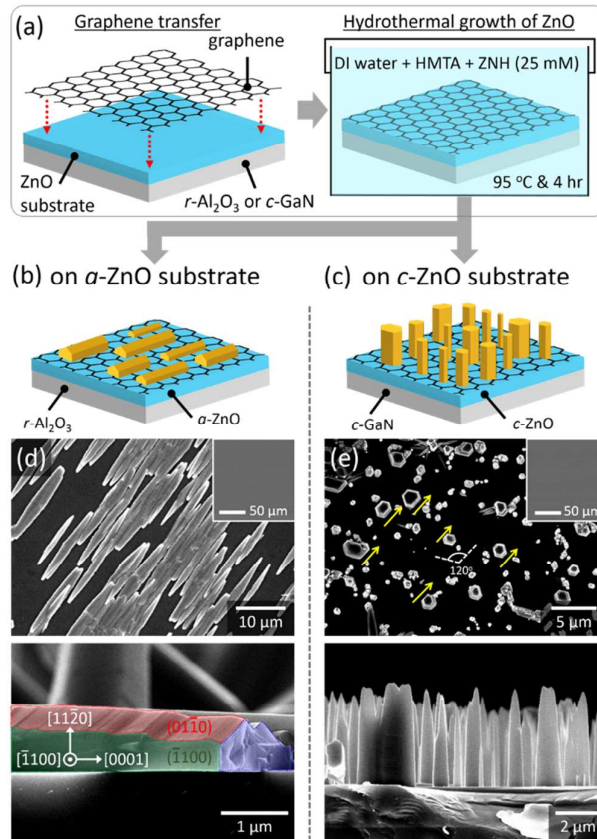


**Fig. 1.** Trans-epitaxial growth of ZnO MRs on graphene-coated ZnO substrates. (a) Schematic illustration depicting the procedures for hydrothermal trans-epitaxy. Illustrations of ZnO MRs trans-epitaxially grown on (b)  $\alpha\text{-ZnO}$  and (c)  $c\text{-ZnO}$  substrates across MLG. Top-view (upper panel) and cross-sectional (bottom panel) SEM images of ZnO MRs grown on MLG-coated (d)  $\alpha\text{-ZnO}$  and (e)  $c\text{-ZnO}$  substrates. Insets in upper panels of (d) and (e) are plan-view SEM images of MLG-coated  $\alpha\text{-}$  and  $c\text{-ZnO}$  substrates, respectively, before overlayer growth. The bottom image in (d) is false-colored to represent facets of  $(0001)$ ,  $(\bar{1}100)$ , and  $(01\bar{1}0)$  with blue, green, and red, respectively. HMTA and ZNH in (a) denote hexamethylenetetramine and zinc nitrate hexahydrate, respectively.

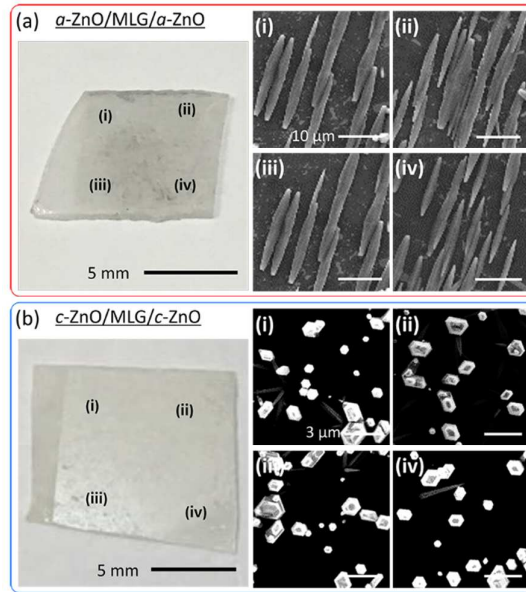


**Fig. 2.** Long-range morphological ordering of trans-epitaxial ZnO MR arrays grown on MLG-coated (a)  $a\text{-ZnO}$  and (b)  $c\text{-ZnO}$  substrate. Left panel is photograph of substrate with a thumbnail size, and right four panels are a series of plan-view SEM images (right) obtained from (i)–(iv) locations marked in the left photograph. For SEM observations, the sample stage was only translationally moved without rotating motion to corroborate the in-plane alignments of MR arrays.

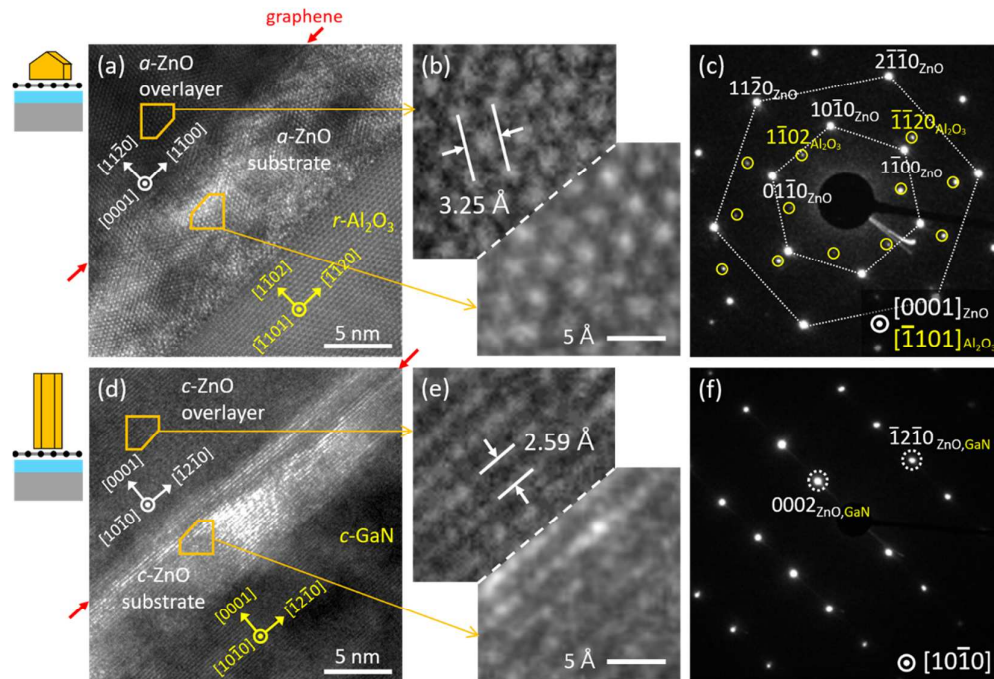


**Fig. 3.** Cross-sectional TEM analyses of trans-epitaxial ZnO MRs/MLG/ZnO substrate. (a) HR-TEM image of horizontal ZnO MR/MLG/*a*-ZnO substrate. (b) The corresponding high-magnification lattice images enlarged from boxed areas of (a). (c) SAED patterns obtained from image of (a). (d) HR-TEM image of vertical ZnO MR/MLG/*c*-ZnO substrate. (e) The corresponding high-magnification lattice images enlarged from the boxed areas of (d). (f) SAED patterns obtained from image (d). The diffraction patterns of (c) and (f) demonstrate the homoepitaxial relationship between the ZnO MR overlayer and substrate across MLG.

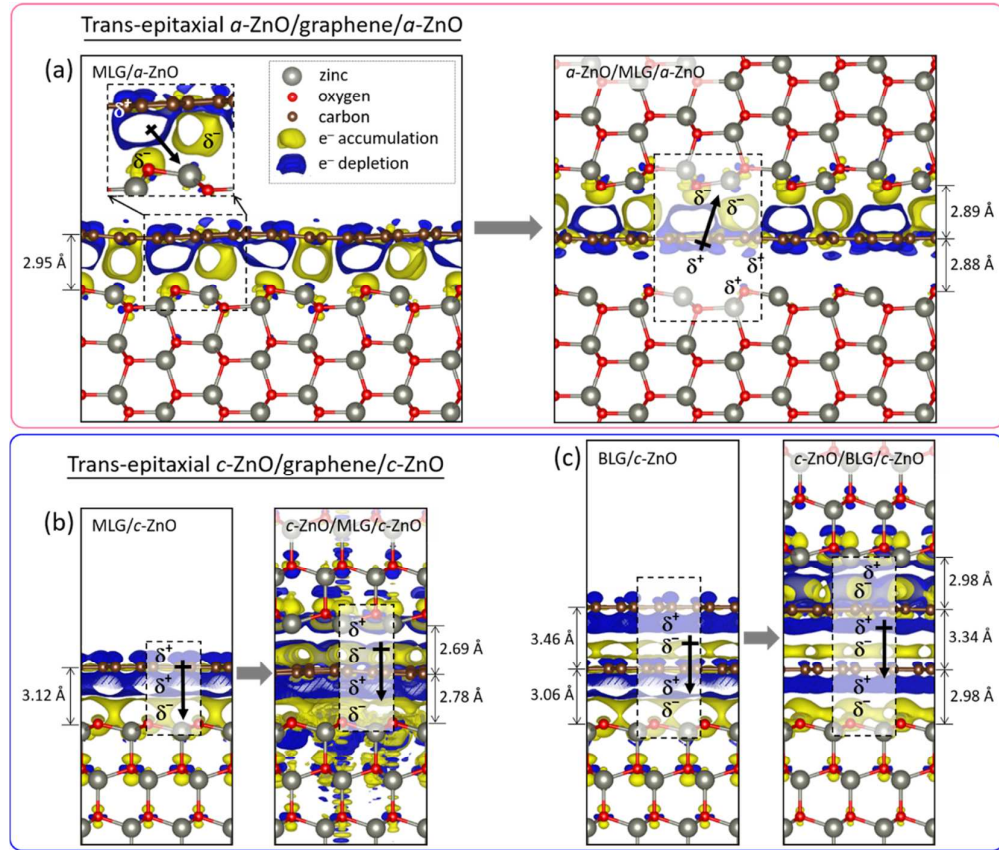


**Fig. 4.** Atomic structure and charge density difference ( $\Delta$ CD) of trans-epitaxial (a)  $\alpha$ -ZnO/MLG/ $\alpha$ -ZnO, (b)  $c$ -ZnO/MLG/ $c$ -ZnO, and (c)  $c$ -ZnO/BLG/ $c$ -ZnO heterointerfaces. All the left panels show stable atomic configuration and  $\Delta$ CD of substrates before trans-epitaxy, while the right panels correspond to those of trans-epitaxial heterointerfaces after the overlayer growth. The  $\Delta$ CDs were depicted at isosurface levels of  $\pm 0.0002$  e/bohr<sup>3</sup>. The yellow and blue isosurfaces stand for the electron accumulation and depletion regions, respectively. The dot-line boxes are chosen to represent repeating unit, where partial charges resulting from electron accumulation and depletion are denoted with  $\delta^-$  and  $\delta^+$ , respectively. The bond dipoles of '+ $\rightarrow$ ' marked in the dot-line boxes denotes the electric dipoles with Lewis notation to describe electric field direction and bond polarity.

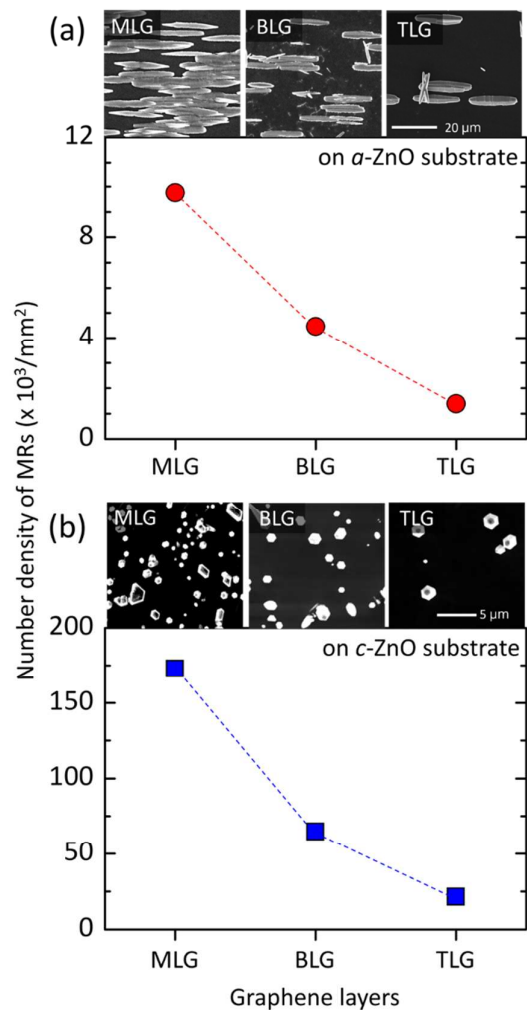


**Fig. 5.** Effect of trans-epitaxial gap and substrate orientation on number density of trans-epitaxial MRs. The number density of (a) horizontal and (b) vertical ZnO MRs, grown on  $\alpha$ - and  $c$ -ZnO substrates, respectively, which was plotted as a function of graphene interlayer thickness that corresponds to trans-epitaxial gap. Insets are a series of plan-view SEM images of MRs grown on different graphene thickness.

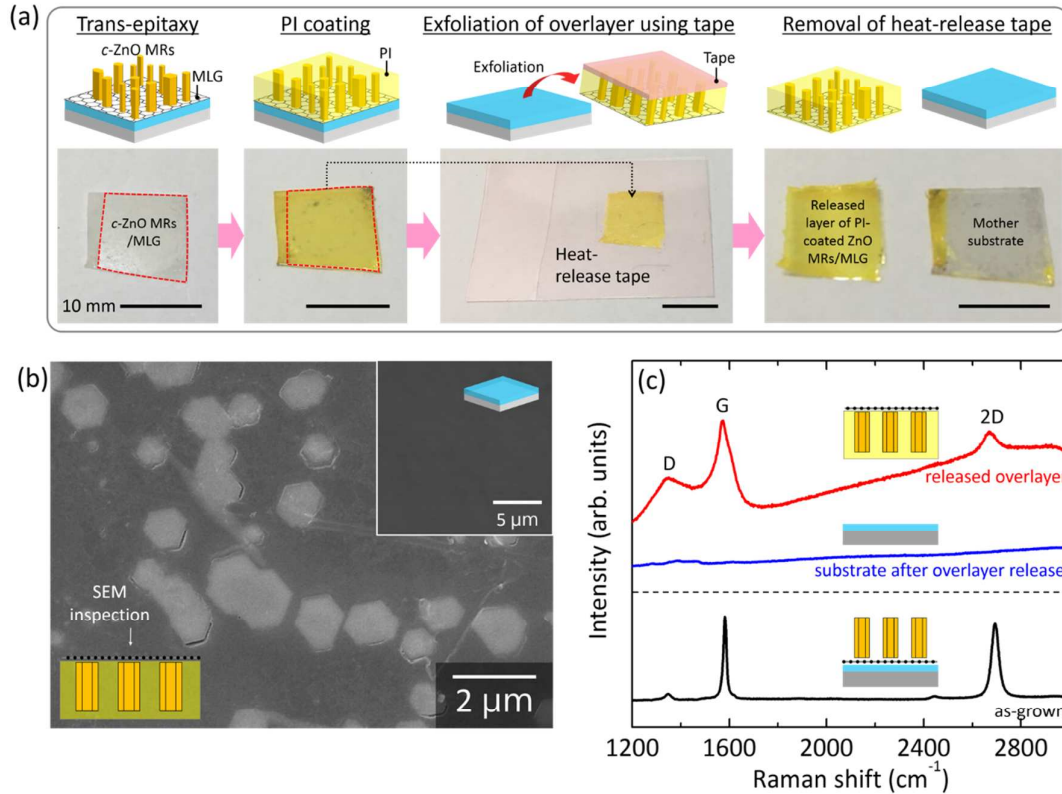


**Fig. 6.** Transferrable trans-epitaxial ZnO MRs overlayer. (a) Schematic illustrations depicting exfoliation process of *c*-ZnO MRs overlayer via PI-supported peeling-off technique using heat-release tape (upper images) and the corresponding photographs displaying the substrate and the released overlayer after each process (lower images). (b) SEM image of the released backside surface of *c*-ZnO MRs supported with PI. Inset SEM image shows the surface of the *c*-ZnO substrate after the exfoliation process. (c) Raman spectra of the as-grown trans-epitaxial *c*-ZnO MRs/graphene/*c*-ZnO substrate before exfoliation (bottom black line), substrate after overlayer release (middle blue line), and the released backside surface of the TLG/PI-filled *c*-ZnO MRs overlayer (top red line).

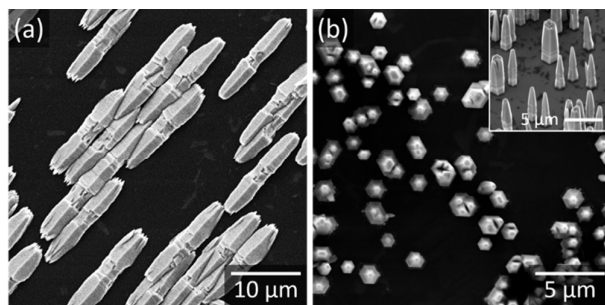


**Fig. 7.** Regeneration of substrate for trans-epitaxy. Plan-view FE-SEM images of ZnO MR arrays grown on reused (a) *a*-ZnO and (b) *c*-ZnO substrates coated with MLG interlayer. Inset in (b) is tilt-view FE-SEM image.

Supplementary Information for

## Trans-epitaxy of ZnO microrods across graphene layers

Junseok Jeong,<sup>¶,†</sup> Kyung-Ah Min,<sup>†, ‡, †</sup> Dong Hoon Shin,<sup>□</sup> Woo Seok Yang,<sup>△</sup> Jinkyung Yoo,<sup>∇</sup> Sang Wook Lee,<sup>□</sup> Suklyun Hong,<sup>\*, †, ‡, †</sup> and Young Joon Hong<sup>\*, †, †</sup>

<sup>¶</sup>Department of Nanotechnology & Advanced Materials Engineering, <sup>†</sup>Graphene Research Institute–Texas Photonics Center International Research Center (GRI–TPC IRC), <sup>‡</sup>Graphene Research Institute, <sup>‡</sup>Department of Physics and Astronomy, Sejong University, Seoul 05006, Republic of Korea

<sup>□</sup>Department of Physics, Ewha Womans University, Seoul 03760, Republic of Korea

<sup>△</sup>Nano Materials Research Center, Korea Electronics Technology Institute, Seongnam, Gyeonggi-do 13509, Republic of Korea

<sup>∇</sup>Center for integrated Nanotechnologies, Los Alamos National Laboratory, Los Alamos, NM 87545, United States

### ■ AUTHOR INFORMATION

#### Corresponding Authors

\*E-mail: [hong@sejong.ac.kr](mailto:hong@sejong.ac.kr) (S.H.); [yjhong@sejong.ac.kr](mailto:yjhong@sejong.ac.kr) (Y.J.H.)

#### Author Contributions

J.J and K-A.M. contributed equally to this work.

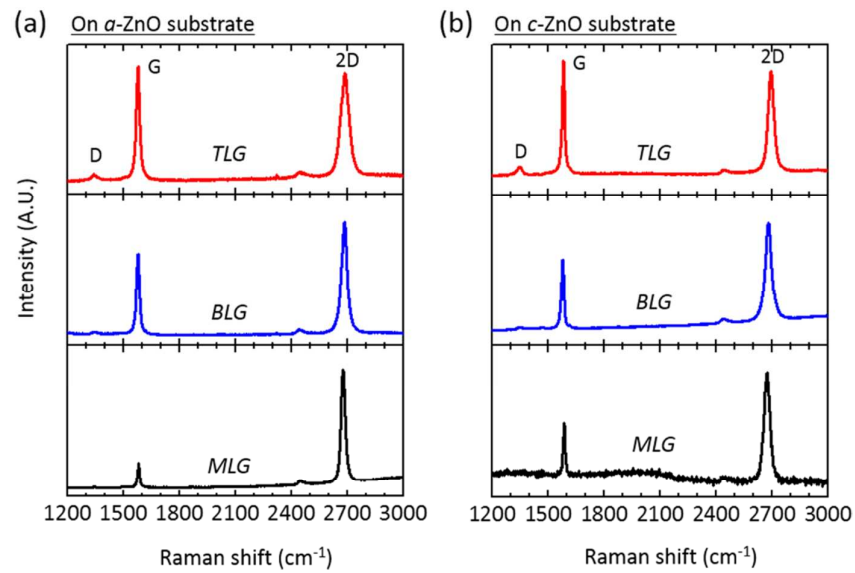


**Figure S1.** Raman spectra for MLG (bottom), BLG (middle), and TLG (top) layers coated on (a)  $\alpha$ -ZnO and (b)  $c$ -ZnO substrates after trans-epitaxy of ZnO overlayer.

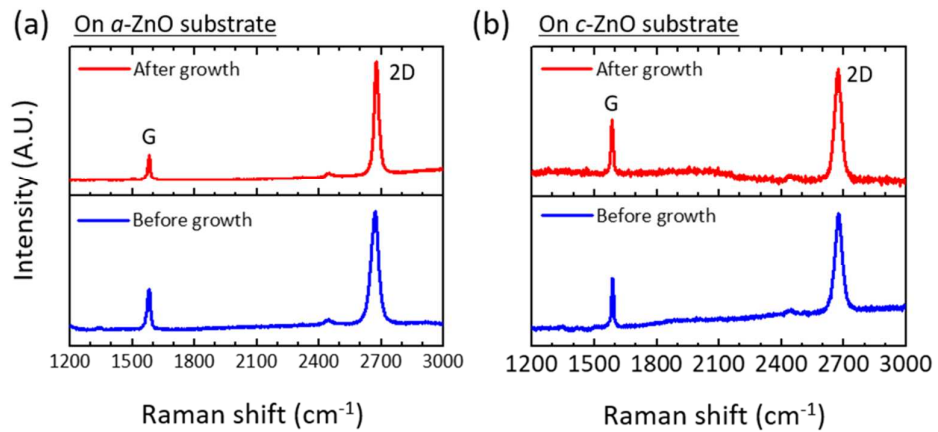


**Figure S2.** Raman spectra for MLG coated on (a)  $\alpha$ -ZnO and (b)  $c$ -ZnO substrates. Bottom blue lines are the spectra obtained before hydrothermal growth of ZnO MRs, and red ones are after hydrothermal growth of ZnO MRs.

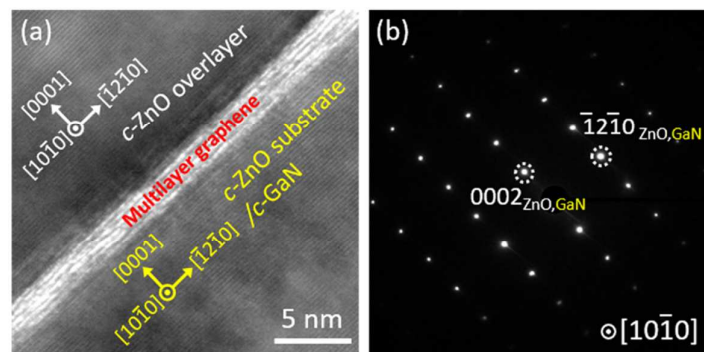


**Figure S3.** Cross-sectional TEM analyses for trans-epitaxial *c*-ZnO/multilayer graphene/*c*-ZnO heterostructure. (a) HR-TEM image. (b) Electron diffraction pattern of *c*-ZnO MR/multilayer graphene/*c*-ZnO substrate.

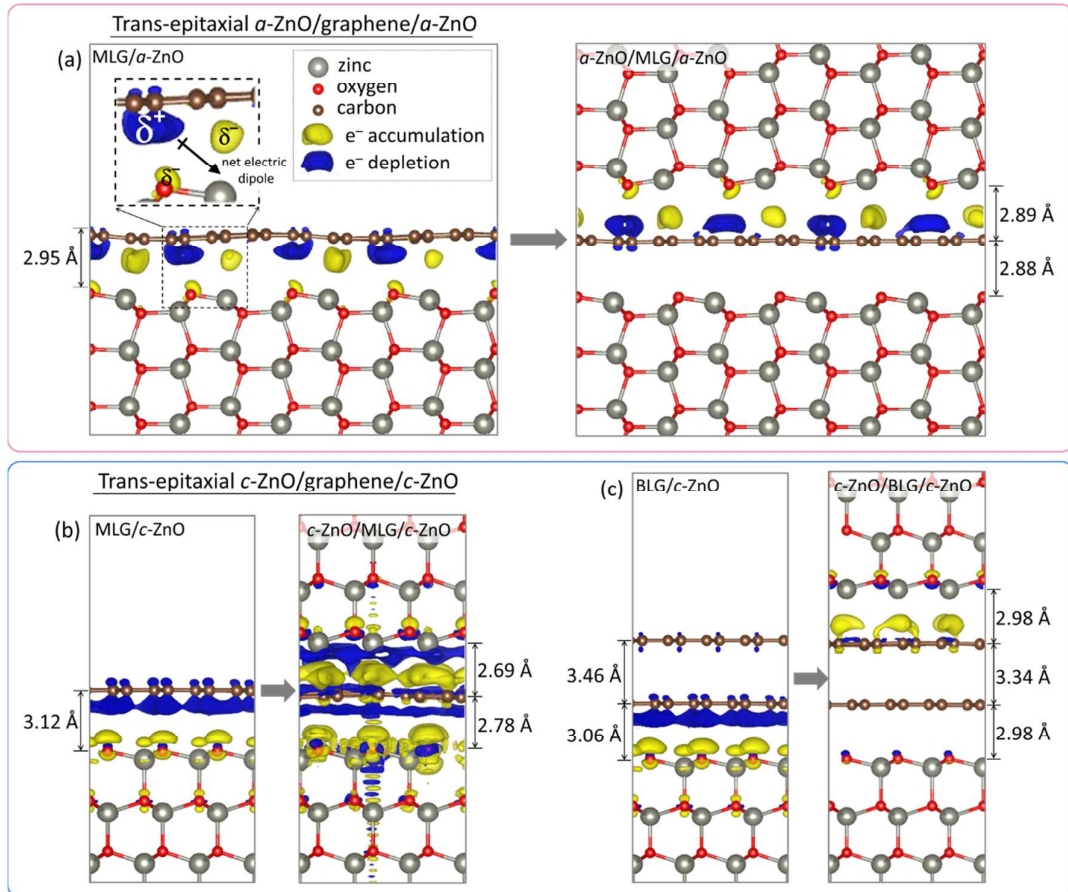


**Figure S4.** Atomic structure and charge density difference ( $\Delta CD$ ) of trans-epitaxial (a)  $\alpha$ -ZnO/MLG/ $\alpha$ -ZnO, (b)  $c$ -ZnO/MLG/ $c$ -ZnO, and (c)  $c$ -ZnO/BLG/ $c$ -ZnO heterointerfaces. All the left panels show stable atomic configuration and  $\Delta CD$  of substrates before trans-epitaxy, while the right panels correspond to those of trans-epitaxial heterointerfaces after the overlayer growth. The  $\Delta CD$ s were depicted at isosurface levels of  $\pm 0.001$  e/bohr<sup>3</sup>. The yellow and blue isosurfaces stand for the electron accumulation and depletion regions, respectively.

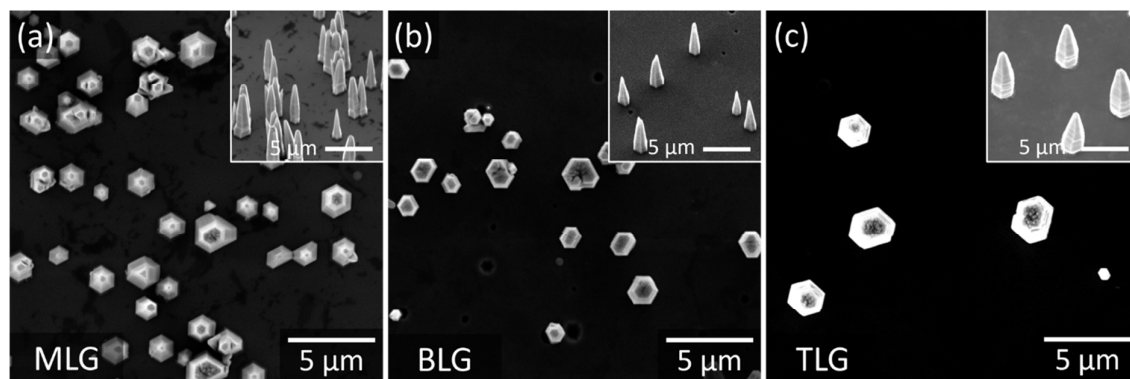


**Figure S5.** Regeneration of substrate for trans-epitaxy of ZnO MRs. Plan-view FE-SEM images of ZnO MR arrays grown on (a) MLG-, (b) BLG-, and (c) TLG-coated *c*-ZnO s substrates. Insets are tilt-view FE-SEM images.